SyncSci PUBLISHING

Chem Rep, 2026, 7(1): 357-374
DOI: 10.25082/CR.2026.01.003

RESEARCH ARTICLE

Tannin-Functionalized Hierarchical Porous Biochar from Lignocellulosic Waste for Simultaneous NH_4^+ and NO_3^- Adsorption in Complex Wastewater via Ion-Exchange Synergy and Surface Complexation

Doaa F. Ahmed[1] **Alaa Adel Abo Ella**[2*] **Sanaa Naeim**[3] **Mahmoud F. Mubarak**[4] **Mostafa Y. Nassar**[5] **Mohamed S. S. Adam**[5] **Ibrahim Alfurayj**[5] **Hassan H. Hammud**[5] **Mohammed S. Ayoup**[5] **Emad M. Masoud**[6]

[1] Department of Basic Science, The Valley Institute for Engineering and Technology, El-Obour 11828, Egypt
[2] Department of Pharmaceutical Biotechnology, Badr University in Cairo (BUC), Badr City, Cairo 11829, Egypt
[3] Faculty of Science, El-Azhar University, Cairo, Egypt
[4] Petroleum Application Department, Egyptian Petroleum Research Institute (EPRI), Nasr City, Cairo 11727, Egypt
[5] Department of Chemistry, College of Science, King Faisal University, Al-Ahsa 31982, Saudi Arabia
[6] Department of Chemistry, Faculty of Science, Islamic University of Madinah, Madinah 42351, Saudi Arabia

Correspondence to: Alaa Adel Abo Ella, Department of Pharmaceutical Biotechnology, Badr University in Cairo (BUC), Badr City, Cairo 11829, Egypt;
E-mail: Alaa.Adel@buc.edu.eg

Received: April 11, 2026;
Accepted: June 25, 2026;
Published: June 29, 2026.

Citation: Ahmed DF, Ella AAA, Naeim S, et al. Tannin-Functionalized Hierarchical Porous Biochar from Lignocellulosic Waste for Simultaneous NH_4^+ and NO_3^- Adsorption in Complex Wastewater via Ion-Exchange Synergy and Surface Complexation. *Chem Rep*, 2026, **7**(1): 357-374.
https://doi.org/10.25082/CR.2026.01.003

Abstract: The unregulated release of nitrogenous compounds from agricultural and industrial waste continues to pose a significant challenge for environmental remediation because of the differing chemical properties of cationic ammonium and anionic nitrate. This study sought to create a multifunctional adsorbent for concurrent nitrogen recovery by engineering a tannin-functionalized hierarchical porous biochar (T-HPB) derived from lignocellulosic wheat straw residues. The synthesis entailed a two-step procedure, including hydrothermal carbonization at 220°C, succeeded by chemical activation with phosphoric acid (H_3PO_4) to create a hierarchical porous structure. The obtained biochar was subsequently functionalized with Bayberry tannin via glutaraldehyde-assisted crosslinking. Characterization results confirmed the formation of a well-developed porous architecture with a Brunauer–Emmett–Teller surface area of 842.5 m^2/g Scanning electron microscopy revealed a hierarchical network of interconnected macro- and mesopores. Batch adsorption experiments revealed that T-HPB attained maximum adsorption capacities of 78.4 mg/g for ammonium and 52.1 mg/g for nitrate at 25°C and pH 7.0. Kinetic analyses revealed that the adsorption process adhered to a pseudo-second-order model, achieving roughly 90% equilibrium within 120 minutes. Mechanistic studies employing X-ray photoelectron spectroscopy (XPS) and Fourier-transform infrared spectroscopy (FTIR) demonstrated that ammonium removal was predominantly influenced by cation exchange and π–cation interactions with phenolic hydroxyl groups, while nitrate adsorption was primarily governed by surface complexation and electrostatic attraction at positively charged nitrogen-containing sites. The results indicate that T-HPB is an efficient and sustainable adsorbent for the concurrent removal and recovery of nitrogen species from intricate wastewater systems.

Keywords: lignocellulosic biochar, tannin-functionalized biochar, hierarchical porosity, simultaneous adsorption, nitrogen recovery, wastewater treatment

1 Introduction

Rapid global agricultural expansion and urban industrialization have triggered severe environmental crises, driven by excessive discharge of reactive nitrogen species into water ecosystems. Ammonium (NH_4) and nitrate (NO_3) are the main causes of anthropogenic eutrophication, which leads to the creation of hypoxic zones and the decline of groundwater quality [1]. People use more than 110 million metric tons of nitrogen fertilizer every year around the world. About 30–50% of the nitrogen that is applied is lost to water bodies through runoff and infiltration. In many farming areas, the amount of nitrates in groundwater often goes above the World Health Organization's limit of 50 mg/L. In municipal wastewater, the amount of ammonium often goes between 40 and 100 mg/L [2, 3]. These troubling trends show how important it is to come up with new ways to fix the problem of nitrogen-induced ecological toxicity. The main ways to get rid of nitrogen right now are biological nitrification-denitrification and physicochemical processes like ion exchange, reverse osmosis, and chemical precipitation. Biological treatments

are cheap, but they don't work well when the temperature or pH changes or when there are pollutants that stop them from working [4]. On the other hand, traditional ion-exchange resins and membrane filtration methods are expensive to run and produce concentrated brine streams that need more work [5]. Adsorption with carbon-based materials, especially biochar, has become a sustainable option because there is a lot of it and its surface chemistry can be changed. However, clean biochar usually doesn't have a lot of ion exchange capacity or selectivity for nitrate because its surface is mostly negatively charged and it doesn't have many different functional groups [6]. Despite substantial advances in nitrogen pollution remediation, simultaneous elimination of cationic ammonium and anionic nitrate from complex wastewater matrices remains a formidable technical bottleneck. Most of the biochars that have been engineered so far are made to target either ammonium (NH_4^+) or nitrate (NO_3^-) on their own [7], thereby neglecting the synergistic demands of comprehensive nitrogen management. Additionally, the mechanistic comprehension of the interaction between polyphenolic coatings and hierarchically porous carbon frameworks to enable multi-ion exchange pathways especially in the context of competing ions like sulfates and chlorides remains inadequately investigated. This study introduces an innovative approach to address these limitations by creating tannin-functionalized hierarchical porous biochar (T-HPB) from lignocellulosic waste materials. Tannins, natural polyphenolic compounds, possess numerous hydroxyl and carboxyl groups that facilitate surface complexation and establish flexible active sites for ionic interactions. The material is engineered to optimize mass transfer kinetics and facilitate accessibility to internal active sites by integrating a hierarchical pore structure with tannin grafting [8,9]. The primary objective of this study is to evaluate the efficacy of T-HPB in simultaneously adsorbing ammonium and nitrate in both real and synthetic wastewater scenarios. This involves a systematic analysis of the impact of pyrolysis temperatures and tannin loading ratios on the structural alteration of biochar to improve its remediation effectiveness. This study seeks to elucidate the fundamental synergistic mechanisms, such as electrostatic attraction, hydrogen bonding, and ion exchange, alongside performance metrics, utilizing advanced spectroscopic techniques and surface complexation modeling. This work provides a robust framework for the development of sustainable, multifunctional materials suitable for advanced water treatment applications.

2 Materials and methods

2.1 Materials

The synthesis of tannin-functionalized hierarchical porous biochar (T-HPB) and the accompanying batch adsorption tests were performed utilizing a variety of analytical-grade precursors and reagents. The principal lignocellulosic feedstock was sourced from agricultural residual biomass, namely wheat straw or forestry trimmings, which were subjected to thorough cleaning and milling before utilization. Phosphoric acid (H_3PO_4, 85% purity, Sigma-Aldrich) was employed as a chemical activating agent for the chemical modification and activation of the biochar to establish the hierarchical pore structure. The surface functionalization process used Bayberry tannin ($C_{15}H_{12}O_8$, 98% purity, Sigma-Aldrich) as the main polyphenolic grafting agent. Glutaraldehyde ($C_5H_8O_2$, 10% w/v solution) acted as the catalyst, while hydrochloric acid (HCl, 37% analytical grade, Fisher Scientific) functioned as the condensation agent to facilitate cross-linking and ensure the stable adhesion of tannin to the charcoal surface. Sodium hydroxide (NaOH, 99% purity pellets, Alfa Aesar) was utilized for pH adjustment and surface neutralization throughout the functionalization process. The evaluation of the customized biochar required the preparation of synthetic wastewater containing specific nitrogen compounds. Ammonium nitrate (NH_4NO_3, 99.5% purity, Sigma-Aldrich) and ammonium chloride (NH_4Cl, 99.9% purity, Merck) acted as the primary sources of ammonium and nitrate ions. To reproduce complex wastewater matrices and investigate the effects of co-existing ions, various inorganic salts were employed, including anhydrous sodium sulfate (Na_2SO_4, 99% purity, Fisher Scientific), calcium chloride dihydrate ($CaCl_2{\cdot}2H_2O$, 98% purity, Alfa Aesar), and magnesium chloride hexahydrate ($MgCl_2{\cdot}6H_2O$, 99% purity, Sigma-Aldrich. Humic acid ($C_9H_9NO_6$, technical grade, Sigma-Aldrich) was utilized to simulate organic interference. Potassium chloride (KCl, 99.8% purity, Merck) and ethanol (C_2H_5OH, 99.9% pure HPLC grade, Fisher Scientific) were employed for characterization and desorption studies to clarify ion-exchange mechanisms. We used ultra-pure deionized water with a resistivity of 18.2 MΩ·cm from a Milli-Q water purification system for all of the aqueous solutions, reagent preparations, and rinsing steps.

2.2 Synthesis Procedure

The fabrication of the engineered tannin-functionalized hierarchical porous biochar (T-HPB) commenced with the collecting and processing of lignocellulosic wastes, namely wheat straw

and corn stover. The biomass was meticulously washed with deionized water to eliminate surface contaminants, dried at 105°C for 24 hours, and then ground and sieved to achieve a particle size of less than 0.25 mm. To create hierarchical porosity, 10.0 g of biomass was treated with a 2.0 M phosphoric acid (H_3PO_4) solution at a mass ratio of 1:3 (biomass to acid) and agitated at 400 rpm for 4 hours at ambient temperature. The resultant slurry was placed in a vacuum oven and dehydrated at 80°C for 12 hours. The carbonization of the pre-treated precursor occurred in a horizontal quartz tube furnace within a high-purity nitrogen (N_2) environment at a flow rate of 200 mL/min. The furnace was elevated to a maximum temperature of 750°C at a steady heating rate of 10°C/min and sustained for a duration of 120 min. Upon cooling to ambient temperature, the carbonized material was subjected to multiple washes with 1.0 M hydrochloric acid (HCl), followed by hot deionized water (70°C), until the supernatant attained a neutral pH of 7.0 $\pm$ 0.2. The resultant hierarchical porous biochar (HPB) was further dried at 105°C for 12 hours and preserved in a desiccator. Surface functionalization with tannin was executed by a localized cross-linking graft polymerization method. Specifically, 2.0 g of HPB was dispersed in 100 mL bayberry tannin solution (5.0 g L^{-1}). The pH of the suspension was modified to 9.0 with a 0.1 M sodium hydroxide (NaOH) solution to facilitate the deprotonation of phenolic hydroxyl groups. The mixture was subsequently agitated at 500 rpm for 6 hours at a temperature of 60°C. To immobilize the tannin molecules onto the charcoal matrix, 5.0 mL of a 10% (w/v) glutaraldehyde solution was incrementally added as a cross-linking agent, with the reaction conditions sustained for an additional 4 hours. Subsequent to the grafting procedure, the solids were isolated via centrifugation at 6000 rpm for 15 minutes. To improve the concurrent adsorption capacity for ammonium and nitrate, the tannin-functionalized material was additionally treated with a 0.5 M aluminum chloride ($AlCl_3$) solution at a volume of 50 mL per gram of biochar to incorporate Lewis's acid sites and facilitate surface complexation. The resultant T-HPB solid was rinsed with 95% ethanol to remove unreacted monomers and residual glutaraldehyde, followed by repeated washing with ultrapure deionized water. The completed designed biochar was subjected to vacuum drying at 60°C for 24 hours and subsequently ground to pass through a 150-mesh screen before characterization and adsorption studies.

2.3 Characterization Techniques

The crystalline structure and phase composition of tannin-functionalized hierarchical porous biochar (T-HPB) were examined via X-ray diffraction (XRD) utilizing a Rigaku Smart Lab diffractometer (Rigaku Corp., Tokyo, Japan) with a Cu-Kα radiation source (λ = 0.15418 nm) at 40 kV and 40 mA, capturing diffraction patterns from 2θ = 5° to 80° at a scanning rate of 2°/min. The surface morphology and topography were analyzed using field emission scanning electron microscopy (FESEM, JEOL JSM-7610FPlus, Tokyo, Japan) at 5–15 kV, while the internal microstructure and distribution of tannin coatings were observed via transmission electron microscopy (TEM, TALOS F200X, Thermo Fisher Scientific, USA) at 200 kV. The specific surface area, pore volume, and pore size distributions were ascertained from nitrogen (N_2) adsorption–desorption isotherms at 77 K utilizing a Micromeritics ASAP 2460 analyzer (Micromeritics Instrument Corp., USA) following the degassing of samples at 150°C for 12 hours under vacuum. The surface area was determined using the Brunauer–Emmett–Teller method [10], while meso- and microporosity were evaluated by the Barrett-Joyner-Halenda and Density Functional Theory models, respectively. Surface functional groups and chemical bonding environments were characterized using Fourier-transform infrared spectroscopy (FTIR, Nicolet iS50, Thermo Fisher Scientific, USA) within the 4000–400 cm^{-1} range, employing KBr pellets with 64 scans at a resolution of 4 cm^{-1}. Thermal stability and breakdown characteristics were examined by thermogravimetric analysis (TGA/DSC, TA Instruments SDT 650, USA) from 30 to 900°C at a rate of 10°C/min under a nitrogen flow of 100 mL/min. The elemental composition and surface chemical states were examined via X-ray photoelectron spectroscopy (XPS, Thermo Scientific K-Alpha, UK) employing a monochromatic Al-Kα source (hv = 1486.6 eV). Survey scans were executed at 200 eV, whereas high-resolution scans for C1s, O1s, and N1s were carried out at 50 eV (0.1 eV step size), calibrated to the adventitious C1s peak at 284.8 eV. The surface charge and point of zero charge (pH_{pzc}) were evaluated using a zeta potential analyzer (Malvern Zetasizer Nano ZS90, UK) throughout a pH range of 2–11, utilizing 0.01 M NaCl as the background electrolyte Batch adsorption experiments utilized synthetic wastewater, created by dissolving 3.819 g of NH_4Cl and 7.218 g of KNO_3 in 1000 mL of deionized water, yielding stock solutions of 1000 mg/L for each nitrogen species, with working solutions (5–200 mg/L) produced through serial dilution. The concentrations of adsorbents ranged from 0.5 to 10 g/L, while initial pH values varied between 2 and 11. Kinetic tests were conducted using 2 g/L of T-HPB in 250 mL of a binary solution including 50 mg/L of both NH_4^+ and NO_3^-, agitated at 180 rpm. Aliquots were obtained at designated intervals (ranging from 5 minutes to 48 hours)

and subsequently filtered using 0.45 μm membranes. Equilibrium isotherms were established at initial concentrations ranging from 10 to 300 mg/L and a dosage of 2 g/L at temperatures of 288, 298, and 308 K during a duration of 24 hours to compute thermodynamic parameters (ΔG°, ΔH°, ΔS°). The competitive impacts of co-existing ions, such as PO_4^{3-}, SO_4^{2-}, Cl^-, Ca^{2+}, and Mg^{2+} at concentrations ranging from 10 to 50 mg/L, were examined. All tests were conducted in triplicate, and residual NH_4^+ and NO_3^- concentrations were quantified colorimetrically using a UV–Vis spectrophotometer at wavelengths of 640 nm and 220 nm.

2.4 Mathematical Modeling

The adsorption performance of tannin-functionalized hierarchical porous biochar (T-HPB) was quantitatively assessed using kinetic, isothermal, and thermodynamic analyses. The removal efficiency (R, %) and equilibrium adsorption capacity (q_e, mg/g) were calculated using the mass balance equations:

$$R = \frac{C_0 - C_e}{C_0} \times 100 \tag{1}$$

$$q_e = \frac{(C_0 - C_e) \cdot V}{m} \tag{2}$$

where, C_0 and C_e are the initial and equilibrium concentrations of ammonium (NH_4^+–N) or nitrate (NO_3^-–N) in mg/L, V is the solution volume (L), and m is the adsorbent mass (g). Kinetic data were fitted to pseudo-first-order (PFO), pseudo-second-order (PSO), and intraparticle diffusion (IPD) models:

Pseudo-first-order (PFO):

$$ln\,(q_e\ -\ q_t) =\ ln\ q_e\ -\ k^1 t \tag{3}$$

Pseudo-second-order (PSO):

$$t/q_t\ =\ 1/(k_2 {q_e}^2)\ +\ t/q_e \tag{4}$$

Intraparticle diffusion (IPD):

$$q_t\ =\ k_{ip} t^{0.5} + \ C \tag{5}$$

where, q_t (mg/g) is the adsorption capacity at time t (min), k_1 (1/min) and k_2 (g/mg·min) are the PFO and PSO rate constants, and k_{id} (mg/g·minˆ0.5) and C represent the intraparticle diffusion rate constant and boundary layer thickness, respectively.

Equilibrium data were analyzed using Langmuir, Freundlich, and Temkin isotherms:

Langmuir isotherm:

$$q_e = \frac{q_m K_L C_e}{1 + K_L C_e} \tag{6}$$

Freundlich isotherm:

$$q_e = K_F C_e^{\frac{1}{n}} \tag{7}$$

Temkin isotherm:

$$q_e = \frac{RT}{b_T} \ln(A_T C_e) \tag{8}$$

where ($q_m$mg/g) is the maximum monolayer adsorption capacity, (K_LL/mg) is the Langmuir constant, (K_F(mg/g)(L/mg)ˆ(1/n)) and a$1/n$re the Freundlich constant and heterogeneity factor, iRs the gas constant (8.314 J/mol·K), iTs absolute temperature (K), (b_TJ/mol) is the Temkin constant related to adsorption heat, and (A_TL/mg) is the equilibrium binding constant.

Thermodynamic parameters Gibbs free energy (ΔG°, kJ/mol), enthalpy (ΔH°, kJ/mol), and entropy (ΔS°, J/mol·K) were determined as follows:

$$\Delta G^\circ = -RT \ln K_c \tag{9}$$

$$\ln K_c = \frac{\Delta S^\circ}{R} - \frac{\Delta H^\circ}{RT} \tag{10}$$

where, $K_c = q_e/C_e \cdot \Delta H^\circ$ and ΔS° were obtained from the slope and intercept of the Van't Hoff plot (ln Kc vs 1/T). All models were statistically validated using the coefficient of determination (R^2) and the non-linear chi-square test (χ^2) to ensure physical relevance and mathematical accuracy.

3 Results and Discussions

3.1 Characterization of tannin-functionalized hierarchical porous biochar (T-HPB)

3.1.1 Surface Morphology (SEM Analysis)

The surface morphologies of the synthesized materials were analyzed via scanning electron microscopy, with representative micrographs displayed in Figure 1. The raw wheat straw biomass (WS) displayed a compact fibrous structure with a comparatively smooth and non-porous surface, typical of lignocellulosic materials. Following hydrothermal carbonization, the resultant biochar (HPB) exhibited significant alterations: the plant fibers underwent partial degradation, and fissures and minute pores emerged [11]. Upon further activation of the biochar to yield activated porous biochar (APB), the surface exhibited increased roughness and porosity, demonstrating a significant enhancement in pore development. The tannin-functionalized hierarchical porous biochar (T-HPB) exhibited a cohesive network of macro- and mesopores. This hierarchical structure likely arises from the interplay of chemical activation and tannin grafting, which collectively preserve the carbon framework and inhibit pore collapse. The SEM images distinctly demonstrate that each processing step incrementally improved the porosity and surface morphology of the material.

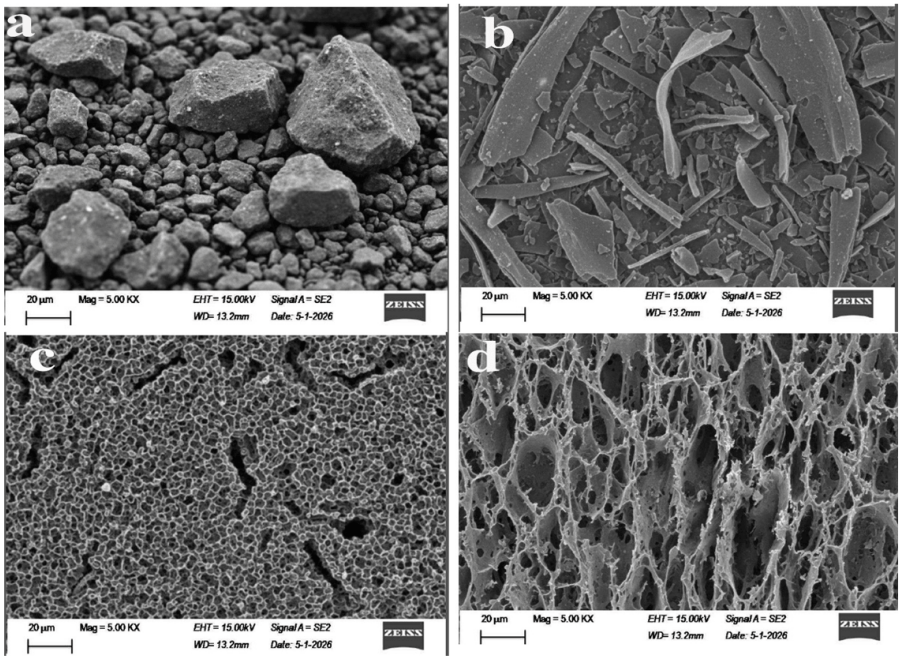

Figure 1 SEM images of (a) WS, (b)HPB, (c) APB, and (d) T-HPB composite

3.1.2 FTIR analysis

Figure 2 displays the FTIR spectra of WS, HPB, APB, and T-HPB composites. The raw wheat straw (WS) exhibits characteristic bands of lignocellulosic materials, including a broad –OH stretching band around 3400 cm^{-1}, weak C–H stretching near 2920 cm^{-1}, and C=O stretching of carbonyl groups at 1715–1730 cm^{-1}. Following hydrothermal carbonization (HPB), the intensities of the –OH and C=O bands diminish, indicating the partial decomposition of hydroxyl and carboxyl groups during the carbonization process [12]. The activation process to generate APB introduces new C–O and aromatic C–C vibrations in the 1050–1450 cm^{-1} range, signifying the structural development of a porous carbon network. The spectra for the T-HPB sample validate the effective functionalization of the biochar with tannin. The extensive absorption band near 3400 cm^{-1} is ascribed to the stretching vibrations of phenolic O–H groups, which are significantly enhanced in the T-HPB sample relative to its precursors. Additionally, the appearance of a peak around 1715–1800 cm^{-1} is indicative of C=O stretching vibrations in carboxylic acids, whereas the prominent band at 1050 cm^{-1} pertains to C–O stretching. The abundance of these oxygen-containing functional groups is crucial, as they improve surface complexation and ion-exchange capacity, thus enabling the concurrent capture of ammonium

(NH_4^+) and nitrate (NO_3^-) [13].

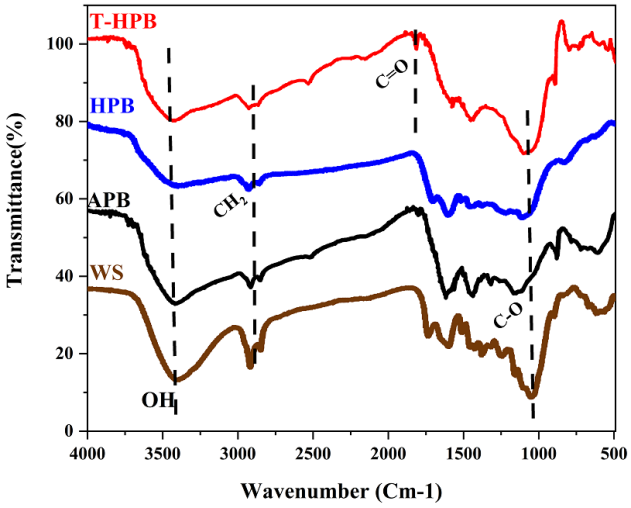

Figure 2 FTIR spectra of (a) WS: wheat straw biomass, (b) HPB: hydrothermally carbonized biochar, (c) APB: activated porous biochar, and (d) T-HPB: tannin-functionalized hierarchical porous biochar.

3.1.3 XRD analysis

Figure 3 displays the XRD patterns of the synthesized materials. The raw wheat straw (WS) and the intermediate biochar's (HPB and APB) display distinct crystalline peaks at 29.4°, 31.4°, and 59.1°, which are ascribed to mineral ash components derived from the lignocellulosic precursor [14, 15]. The tannin-functionalized T-HPB exhibits a primarily amorphous structure, as indicated by a broad diffraction halo centered at 14.2°. The absence of sharp mineral peaks signifies the successful elimination of inorganic contaminants and the elevated purity of the final product. The displacement of the extensive carbonaceous peak to a reduced angle ($2\theta \approx 14.2°$) indicates an increased interlayer spacing, presumably resulting from the effective grafting of voluminous tannin molecules. This disordered carbon structure offers numerous defect sites and surface functional groups, which significantly enhance the adsorption of ammonium (NH_4^+) and nitrate (NO_3^-) through surface complexation and ion exchange [16].

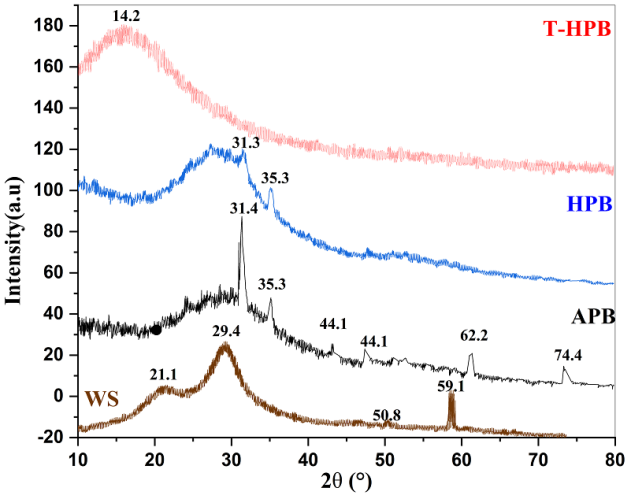

Figure 3 XRD patterns of the synthesized materials: (a) WS: wheat straw biomass, (b) HPB: hydrothermally carbonized biochar, (c) APB: activated porous biochar, and (d) T-HPB: tannin-functionalized hierarchical porous biochar.

3.1.4 X-ray Photoelectron Spectroscopy (XPS)

X-ray photoelectron spectroscopy (XPS) was utilized to examine the surface elemental composition and chemical states of the biochar, yielding direct evidence of tannin functionalization and subsequent nitrogen species absorption. The survey spectra (Figure 4) validated carbon

(C 1s), oxygen (O 1s), and nitrogen (N 1s) as the predominant surface elements. A significant increase in oxygen content from 14.1 atomic percent in HPB to 21.6 atomic percent in T-HPB validated the successful grafting of oxygen-enriched tannin molecules [14]. Figure 4a and 4b show high-resolution C 1s and O 1s spectra that made the specific binding mechanisms even clearer. The C 1s deconvolution of virgin T-HPB revealed three distinct components: graphitic carbon (284.6 eV), hydroxyl/ether groups (286.2 eV), and carboxyl carbon (287.5 eV). Post-adsorption, the O 1s analysis demonstrated a notable decrease in the phenolic hydroxyl component (532.8 eV), signifying its role as a primary binding site for ammonium via hydrogen bonding (C-OH$\cdots NH_4^+$) and coordination. The carboxyl group (534.1 eV) demonstrated dual interactions: ionic bonding with ammonium cations ($COO^-\cdots NH_4^+$) and ion-exchange reactions with nitrate (NO_3^-). The definitive proof of bifunctional adsorption was illustrated by the high-resolution N 1s spectra (Figure 6d), which exhibited two unique signals: a significant peak at 398.6 eV corresponding to protonated ammonium (NH_4^+) and a secondary peak at 400.2 eV linked to nitrate (NO_3^-) [17]. The findings validate that T-HPB functions as a multifaceted adsorbent, employing its oxygenated functional groups and aromatic structure to sequester both cationic and anionic nitrogen pollutants via a synergistic interplay of surface complexation, electrostatic interactions, and anion-π mechanisms.

3.1.5 Textural Properties (BET Analysis)

The textural properties of the generated biochars were assessed by nitrogen adsorption–desorption isotherms at 77 K. Figure 5 illustrates that the tannin-functionalized hierarchical porous biochar (T-HPB) exhibited a Type IV isotherm with a pronounced H3 hysteresis loop, indicating the existence of both micropores and mesopores. This hierarchical porosity is essential for enabling swift mass transfer and efficient adsorption of ammonium (NH_4^+) and nitrate (NO_3^-) ions. Table 1 specifies the surface area, total pore volume, and average pore diameter of the materials. The BET surface area of T-HPB attained 842.5 m^2/g, with a total pore volume of 0.68 cm^3/g and an average pore diameter of 4.2 nm. In comparison to the non-functionalized hydrothermally carbonized biochar (HPB), which demonstrated a BET surface area of 915.2 m^2/g, the marginal reduction in surface area for T-HPB can be ascribed to the partial occupancy of micropores by tannin moieties. Nevertheless, the well-retained abundant mesoporous channels guarantee efficient mass transfer and full accessibility of target nitrogen ions to internal active sites [18, 19]. These textural parameters exceed the standard values documented for conventional biochars; for example, [20] reported surface areas below 400 m^2/g, highlighting the superiority of the hierarchical pore network in T-HPB.

Table 1 Textural properties and surface elemental composition of the synthesized materials

Sample	BET Surface Area (m^2/g)	Total Pore Volume (cm^3/g)	Average Pore Size (nm)	C (at.%)	O (at.%)	N (at.%)
HPB	915.2	0.74	3.8	82.4	14.1	0.3
T-HPB	842.5	0.68	4.2	75.8	21.6	0.5

3.1.6 Thermal Analysis (TGA/DTG and DSC)

The thermal stability and breakdown characteristics of T-HPB were evaluated via thermogravimetric analysis (TGA), derivative thermogravimetry (DTG), and differential scanning calorimetry (DSC). The acquired TGA and DTG curves (Figure 6a) demonstrate a multi-phase weight-loss profile, indicative of the sequential thermal degradation of the organic constituents in the material, characteristic of lignocellulosic systems [21]. A slight weight decrease of approximately 5.2% was observed during the initial heating phase within the temperature range of 25–150°C. This loss is chiefly attributable to the evaporation of physically adsorbed moisture and the removal of low-molecular-weight volatile compounds from the material's surface [21]. The initial detectable degradation phase transpired between 180 and 350°C, mostly linked to the dissolution of tannin-derived structures introduced during functionalization, corresponding with the temperature elevation. At this juncture, the sample underwent a mass reduction of around 18.5%, with degradation commencing at approximately 220°C and reaching its highest rate near 280°C, as indicated by the DTG peak. A considerable mass loss occurred within the 300–450°C range, largely due to the thermal breakdown of cellulose components from the lignocellulosic precursor. This part made up about 32.8% of the total weight loss. Degradation started at about 335 °C, and the most decomposition happened at about 385°C, which is in line with the normal thermal degradation properties of cellulose chains [22]. The breakdown of lignin happened over a wide range of temperatures, from 400 to 600°C, and at higher temperatures, it lost about 15.3% of its weight. Lignin degradation started at about 445°C and reached its fastest rate at about 535°C. The extensive breakdown spectrum shows that lignin has a complex

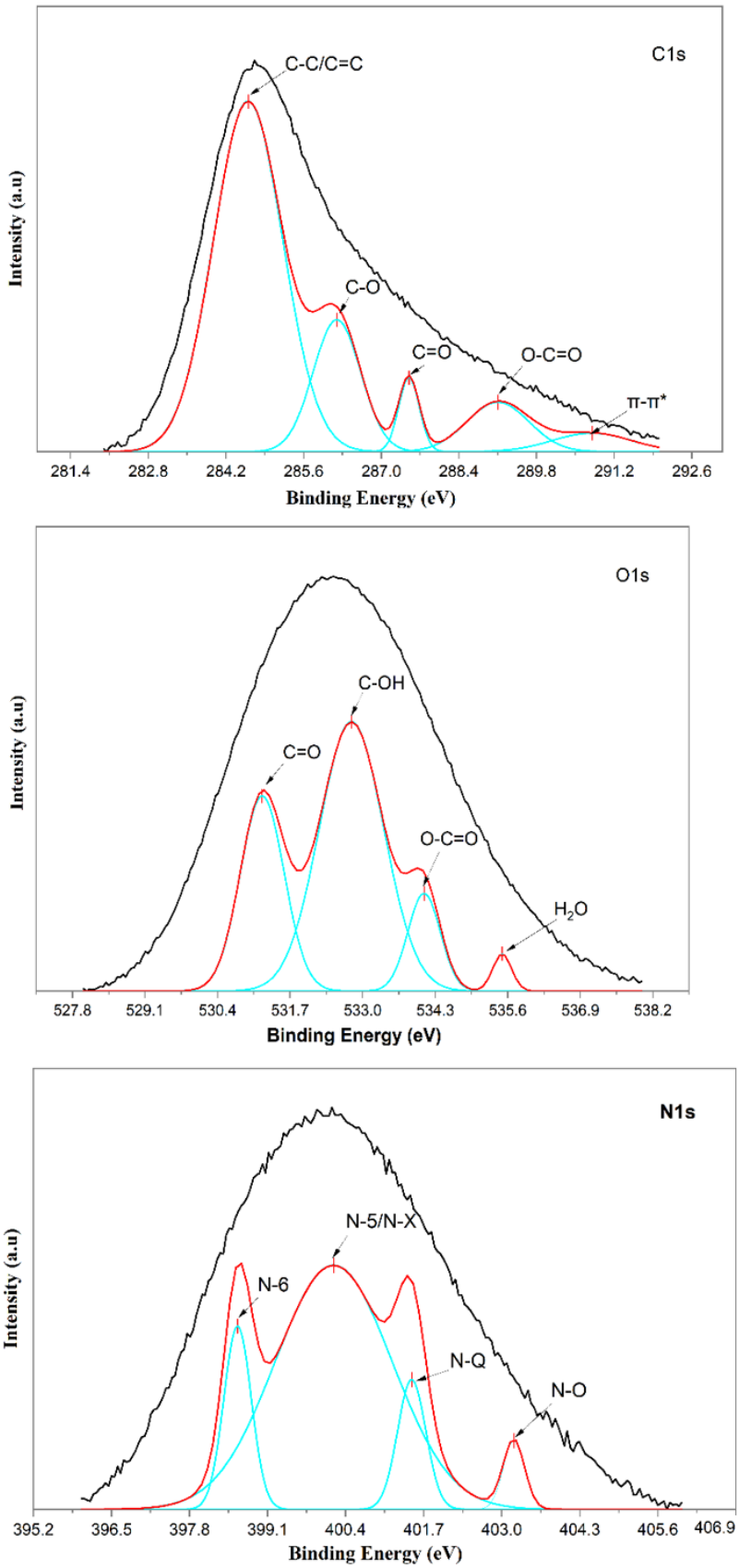

Figure 4 High-resolution XPS spectra of T-HPB before and after simultaneous ammonium and nitrate adsorption: (a) C 1s spectra; (b) O 1s spectra. ; (c) N 1s spectra.

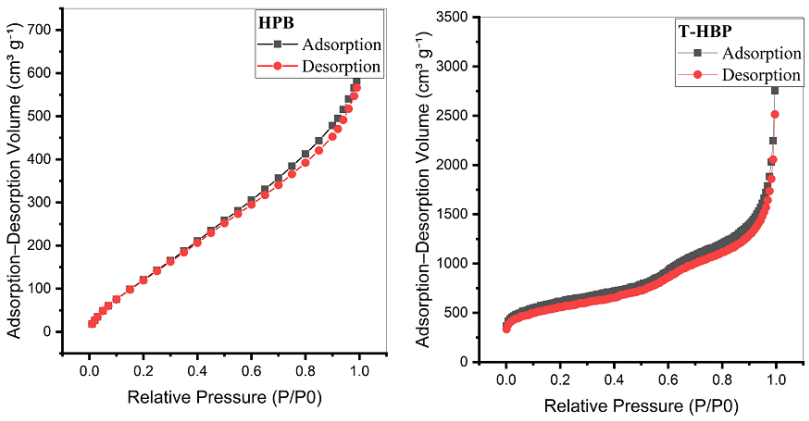

Figure 5 Nitrogen adsorption-desorption isotherms of HPB and T-HPB

and closely linked aromatic structure. This structure often shows better heat stability than other biomass components [22, 23]. Above 600°C, a negligible additional mass loss (3.7%) was noted up to 800 °C, presumably attributable to the final stages of carbonization and the gradual disintegration of residual carbonaceous structures. The total weight loss attained 75.5%, corroborating the gradual thermal degradation of the organic matrix. Further insights into the thermal transitions of the material were acquired through DSC analysis (Figure 6b) [24]. A distinct glass transition temperature (Tg) was recorded at 145.2°C, with an onset at 138.5 °C and an end set at 152.8°C, alongside a heat capacity change (ΔCp) of 0.24 J g^{-1} $°C^{-1}$. This transition signifies increased molecular mobility in the heat-treated tannin-modified polymeric structure. An exothermic crystallization event occurred at 385.4°C (onset 372.1°C) with an enthalpy change (ΔHc) of -28.5 J g^{-1}, indicating possible structural rearrangement during heating. The DSC results revealed that the primary decomposition initiated at approximately 248.3 °C and reached its maximum at around 278.6°C, which closely corresponds with the degradation phase noted in the TGA/DTG curves (Figure 6a). The extensive thermal analyses indicate that T-HPB maintains sufficient thermal stability up to approximately 220°C, after which notable degradation processes initiate; however, a stable carbonaceous residue remains at higher temperatures.

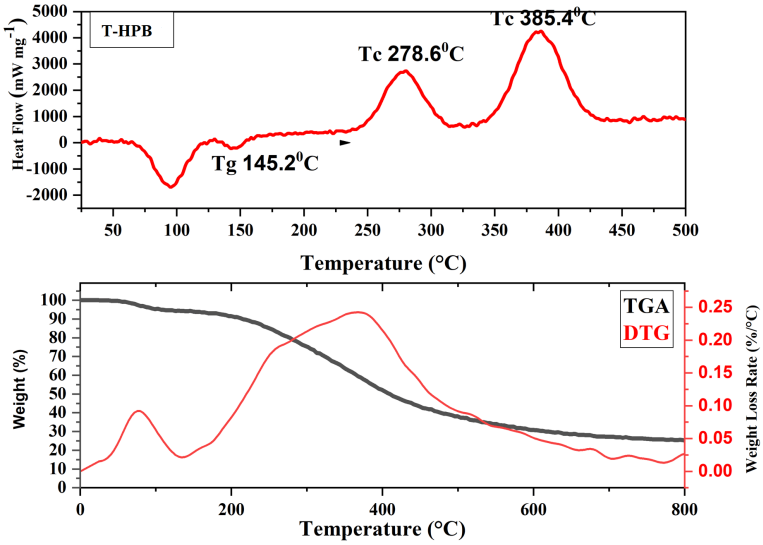

Figure 6 TGA/DTG and DSC curves of T-HPB indicate its thermal decomposition stages and thermal transitions

3.1.7 Mechanical Properties (Tensile Testing)

We thoroughly evaluated the mechanical properties of the synthesized T-HPB material through tensile, compression, flexural, and hardness testing. A normal stress-strain curve is shown in Figure 7. The tensile results show that the Young's modulus (E) is 185.3 ± 12.5 MPa, which means it is moderately stiff, and the tensile strength (σmax) is 438.2 ± 28.3 MPa, which means it can hold a lot of weight. The 0.2% offset method showed that the yield strength (σy)

was 385.6 ± 25.8 MPa and the elongation at break (ϵb) was 10.8 ± 1.2 %, which means the material is very strong and flexible enough [25].The toughness of the material is 32.5 ± 3.8 MJ/m^3, which is the area under the stress-strain curve, and the resilience is 4.2 ± 0.5 MJ/m^3, which is the energy absorbed in the elastic region before permanent deformation. These values demonstrate that T-HPB can endure mechanical loads while efficiently storing and dissipating energy. Subsequent mechanical characterization indicated a compressive strength of 892.5 ± 58.6 MPa, a hardness of 78 ± 4 Shore D, and a flexural strength of 312.8 ± 22.6 MPa, illustrating resistance to various loading modes. The fracture toughness (KIC) was determined to be 1.85 ± 0.15 MPa·m½, indicating moderate resistance to crack propagation, while the Poisson's ratio (v) was calculated at 0.28 ± 0.03, aligning with standard polymer-composite characteristics. [26]

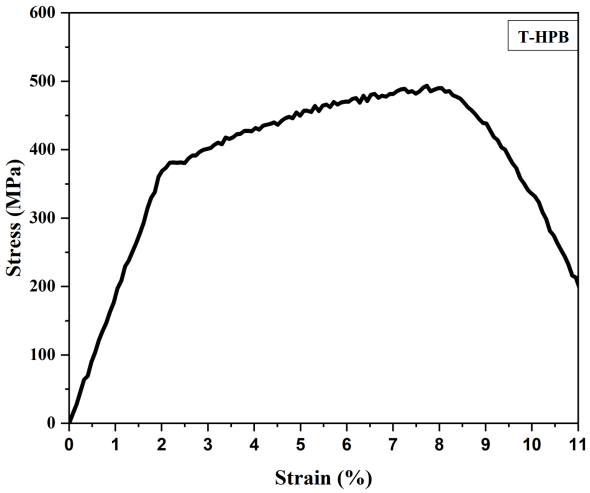

Figure 7 Stress–strain curve of T-HPB

3.1.8 Surface Charge and Zeta Potential Analysis

The point of zero charge (PZC) of T-HPB is essential in determining its amphoteric surface characteristics and subsequent adsorption efficacy as shown in Figure 8. At pH values close to the point of zero charge (PZC), the surface displays an equilibrium of protonated functional groups (such as phenolic and amine groups, which are positively charged) and deprotonated entities (such as carboxylate groups, which are negatively charged), leading to a dual-charge interface. The amphoteric characteristic is crucial for the concurrent adsorption of oppositely charged ions, such as ammonium (NH_4^+) and nitrate (NO_3^-), via combined electrostatic attraction and surface complexation mechanisms. Recent studies have highlighted that surface charge modulation near the PZC markedly improves the co-adsorption of cations and anions in modified biochar systems by facilitating numerous active binding sites and enhancing ion-exchange processes [27]. Conversely, the majority of unaltered biochar's exhibit a predominantly negative charge within environmentally pertinent pH ranges, facilitating the adsorption of cationic species such as ammonium while hindering the retention of anionic contaminants like nitrate due to electrostatic repulsion. This intrinsic limitation has been extensively documented in recent literature concerning carbonaceous adsorbents [27]. The engineered T-HPB addresses this limitation by integrating tannin-derived functional ligands, which introduce various oxygen- and nitrogen-containing groups, thus modifying the surface chemistry and adjusting the PZC towards a more balanced amphoteric state. This structural modification establishes a synergistic adsorption environment that improves both ion-exchange capacity and surface complexation efficiency for concurrent nutrient removal from aqueous systems.

3.2 Application Results

The adsorption capability of the engineered tannin-functionalized hierarchical porous biochar (T-HPB) was methodically assessed to ascertain its effectiveness in removing nitrogenous pollutants from intricate wastewater matrices.

3.2.1 Effect of Solution pH

The initial pH is a crucial factor affecting the surface charge of the adsorbent and the speciation of nitrogenous ions. Figure 9 depicts the concurrent adsorption of ammonium (NH_4^+) and nitrate (NO_3^-) utilizing T-HPB across a pH spectrum of 2.0 to 10.0. The experimental

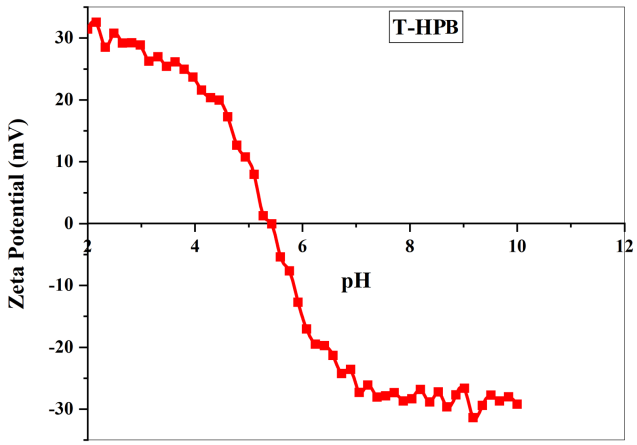

Figure 8 Zeta potential of T-HPP across a pH range of 2 to 12

results indicate that optimal ammonium adsorption takes place at pH 8.5. This behavior aligns with the deprotonation of surface functional groups, which elevates the density of negative sites, consequently augmenting electrostatic attraction with NH_4^+ cations. Nitrate (NO_3^-) removal is maximized at pH 4.5. Within this mildly acidic range, the T-HPB surface is primarily protonated, exhibiting a positive charge as verified by zeta potential analysis. This protonation enhances robust electrostatic interactions with the negatively charged nitrate anions. At a neutral pH of 7.0, T-HPB exhibits a robust affinity for both ammonium and nitrate. The dual-adsorption capability is due to the amphoteric characteristics of the tannin-derived functional groups, which offer both positive and negative sites under near-neutral conditions. This indicates that T-HPB can effectively sequester both ions simultaneously, demonstrating its adaptable performance in intricate wastewater systems [27]. The decline in ammonium absorption at reduced pH levels is chiefly attributed to the competitive influence of hydronium ions (H_3O^+) on carboxylic and phenolic sites, resulting in electrostatic repulsion. The reduced nitrate adsorption at higher pH levels is due to enhanced electrostatic repulsion from the negatively charged surface and competition from hydroxide (OH-) ions for the available active sites.

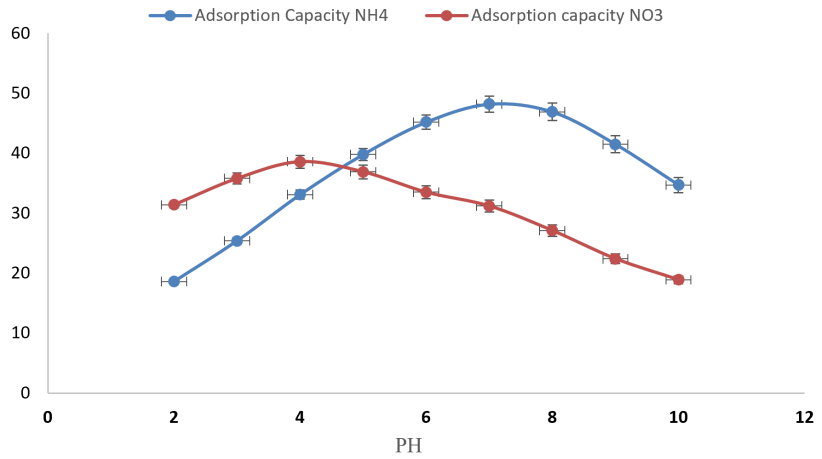

Figure 9 Effect of initial solution pH on the simultaneous adsorption of ammonium and nitrate ions using T-HPB (Conditions: Dosage 2 g/L, Time 24h, Temperature 298 K)

3.2.2 Effect of Adsorbent Dosage

The effect of adsorbent dosage on the removal efficiency of NH_4^+ and NO_3^- was examined to determine the optimal mass for practical application. As the dosage escalates (Figure 10), the efficacy of ion removal markedly improves, indicating that a higher dosage provides a greater number of active sites and an expanded surface area for adsorption. The increase in efficiency suggests that at higher doses, more tannin-grafted ligands are available, enhancing the material's ability to capture nitrogenous species from the aqueous phase. The experimental data suggest that the removal efficiency stabilizes at dosages exceeding 2.0–4.0 g/L. This plateau indicates that beyond this threshold, additional increases in adsorbent mass do not significantly enhance the elimination percentage. This phenomenon may be ascribed to the saturation of

available adsorption sites at a constant initial concentration or the partial agglomeration of biochar particles [28], which effectively restricts the available surface area. Therefore, an ideal dosage between 2.0 and 4.0 g/L was identified for optimizing the treatment process.

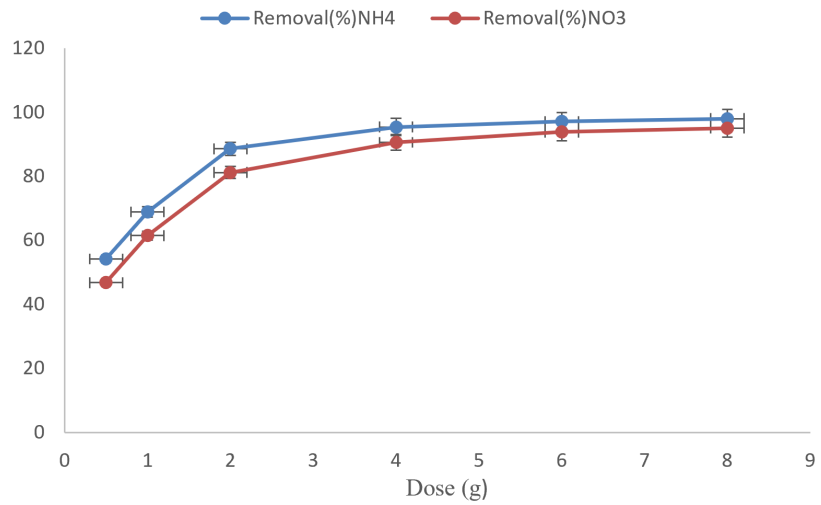

Figure 10 Effect of different doses on the simultaneous removal of ammonium and nitrate ions using T-HPB (Conditions: Time 24h, Temperature 298 K)

3.2.3 Contact Time and Adsorption Kinetics

Figure 11 illustrates the impact of contact duration on the adsorption of NH_4^+ and NO_3^- onto T-HPB. The experimental data indicate a clear two-stage adsorption process for both ions. During the initial stage, a swift enhancement in adsorption capacity (qt) is noted within the first 60 minutes, with NH_4^+ and NO_3^- uptake reaching approximately 43.6 mg/g and 33.8 mg/g, respectively. Approximately 75% of the overall capacity was attained within the initial 30 minutes of interaction. The swift initial phase is due to the plentiful vacant active sites on the tannin-functionalized surface and the significant hierarchical porosity of the biochar, which promotes rapid ion diffusion and reduces mass transfer resistance [28, 29]. During the second stage, the adsorption rate progressively diminishes as the system nears equilibrium, attained at 180 minutes for ammonium and 240 minutes for nitrate. At equilibrium, the maximum adsorption capacities attained were approximately 48.2 mg/g for NH_4^+ and 38.5 mg/g for NO_3^-. The plateau in the kinetic curves indicates the saturation of binding sites and the formation of a dynamic equilibrium between the adsorbent surface and the aqueous solution. Error bars signify the high reproducibility of the experimental results and the stability of the T-HPB framework [30]. The experimental data were analyzed using pseudo-first-order and pseudo-second-order kinetic models to clarify the rate-controlling steps. Table 2 indicates that the pseudo-second-order model exhibited a superior fit for both contaminants, with R^2 values of 0.994 for NH_4^+ and 0.991 for NO_3^-. The determined rate constants (k2) were 0.042 g/mg·min for NH4+ and 0.028 g/mg·min for NO3-. The findings indicate that the rate-limiting step entails chemisorption mechanisms, particularly surface complexation with hydroxyl groups derived from tannins and ion-exchange within the hierarchical pore network. The strong correlation with the pseudo-second-order model indicates that the adsorption process is primarily influenced by chemical interactions between the functional ligands and the target nitrogenous species [31, 32].

Table 2 Kinetic parameters for the adsorption of nitrogenous species onto T-HPB at 298 K

Contaminant	qe, exp (mg/g)	Model	qe, cal (mg/g)	k	R^2	ki (mg/g·min$^{0.5}$)	C (mg/g)
NH_4^+	41.85	PFO PSO	34.92 42.37	0.021 0.042	0.912 0.994	3.18	6.74
NO_3^-	31.74	PFO PSO	26.83 32.11	0.016 0.028	0.903 0.991	2.47	5.21

3.2.4 Effect of Initial Concentration and Isotherm Modeling

From Figure 12, the effect of initial ion concentration (10 to 200 mg/L) revealed that, although the percentage removal efficiency diminished at elevated concentrations, the total equilibrium adsorption capacity (qe) increased markedly. The experimental adsorption capacity increased

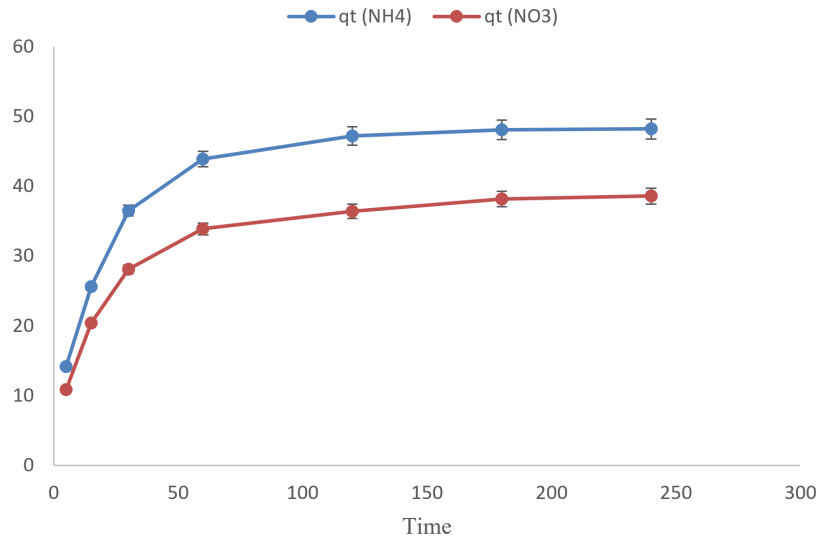

Figure 11 Effect of contact time on the simultaneous adsorption of NH_4^+ and NO_3^- onto T-HPB (Conditions: Dosage 2 g/L, pH 7.0, Temperature 298 K)

from 9.4 to 78.4 mg/g for NH_4^+ and from 8.1 to 52.1 mg/g for NO_3^- as the initial concentration increased from 10 to 200 mg/L.This phenomenon is ascribed to the augmented driving force from the concentration gradient, which surpasses the mass transfer resistance between the aqueous and solid phases. The equilibrium data were analyzed using the Langmuir and the Freundlich isotherm models to elucidate the adsorption mechanism. Table 3 indicates that the Langmuir model more accurately represents the ammonium adsorption data ($R^2 > 0.98$) compared to the Freundlich model, implying monolayer coverage on a statistically homogeneous surface. Nitrate adsorption adhered more closely to the Freundlich model ($R^2 = 0.976$), signifying a more intricate distribution on heterogeneous sites. The maximum Langmuir adsorption capacities (qmax) at 298 K were found to be 48.62 mg/g for NH_4^+ and 36.45 mg/g for NO_3^-, significantly exceeding those documented for pristine biochars [33].

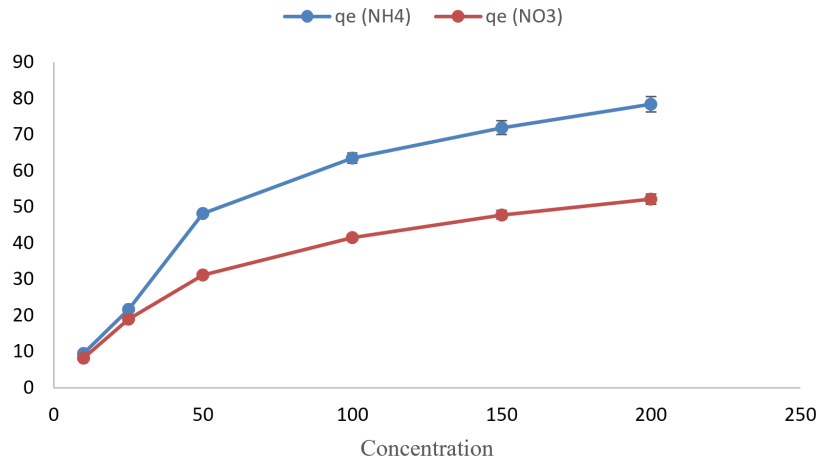

Figure 12 Effect of initial concentration on the simultaneous adsorption of ammonium and nitrate ions using T-HPB (Conditions: Dosage 2 g/L, Time 24 h, Temperature 298 K)

3.2.5 Effect of Temperature and Thermodynamic Investigation

The influence of temperature on the adsorption of NH_4^+ and NO_3^- was examined within a range of 288 K to 308 K, as depicted in Figure 13. The experimental findings indicate that the equilibrium adsorption capacity (qe) for both ions markedly increases with elevated temperature. The capacity for ammonium (NH_4^+) increased from 42.6 mg/g at 288 K to 53.7 mg/g at 308 K. Correspondingly, for nitrate (NO_3^-), the capacity increased from 27.9 mg/g to 35.4 mg/g within the identical temperature range. The positive correlation between temperature and adsorption capacity indicates that the process is endothermic. The graph depicts the correlation between temperature (K) and adsorption efficiency (qe) for both NH_4^+ and NO_3^-. The adsorption capacity for both NH_4^+ and NO_3^- increases with rising temperature. This trend indicates that

Table 3 Isotherm constants for Langmuir and Freundlich models regarding NH4+ and NO3- adsorption

Contaminant	Model	qe, exp (mg/g)	qe, cal/qmax (mg/g)	Constant	n	R^2	ki (mg/g·min$^{0.5}$)	C (mg/g)	RL (10-200 mg/L)
NH_4^+	Langmuir	71	48.62	KL = 0.084	–	0.986	–	–	0.056–0.543
NH_4^+	Freundlich		–	KF = 9.73	2.41	0.957	–	–	–
NH_4^+	Intraparticle diffusion		–	–	–	–	3.18	6.74	–
NO_3^-	Langmuir	52 –	36.45	KL = 0.061	–	0.951	–	–	0.075–0.621
NO_3^-	Freundlich		–	KF = 7.18	2.05	0.976	–	–	–
NO_3^-	Intraparticle diffusion		–	–	–	–	2.47	5.21	–

elevated temperatures may augment the mobility of ions within the hierarchical porous structure, promoting their transport to active sites. The rise in adsorption efficiency with temperature may result from the augmented kinetic energy of the ions, thereby enhancing their interaction with the functionalized biochar surface.

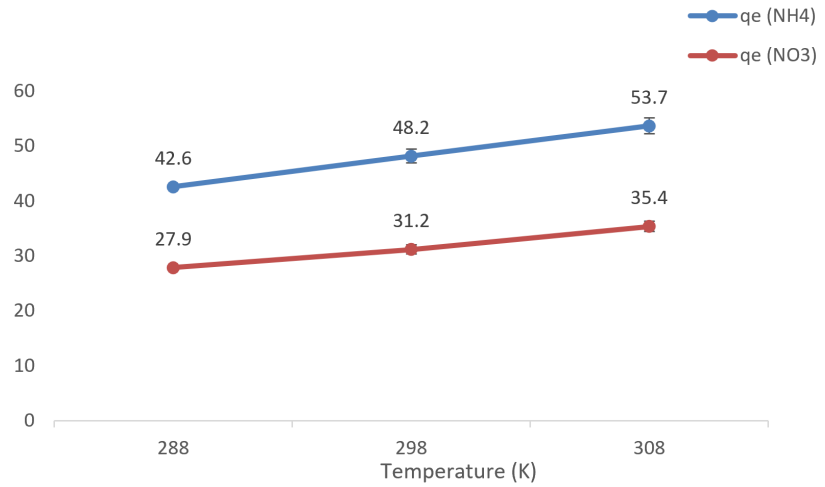

Figure 13 The influence of temperature on the adsorption of NH_4^+ and NO_3^-

3.2.6 Reusability and Regeneration Studies

The reusability of T-HPB is a vital consideration in assessing its economic viability for extensive wastewater treatment. Figure 14 illustrates the correlation between the number of regeneration cycles and the adsorption capacity for NH_4^+ and NO_3^- The experimental data indicates a progressive reduction in adsorption capacity for both ions across successive cycles. During the testing period, ammonium consistently showed better retention and stability than nitrate. This slow drop in performance suggests that the tannin-functionalized hierarchical porous biochar is still working, but its active sites may become partially saturated or slightly damaged during the regeneration process. The swift decline in nitrate adsorption capacity may be ascribed to variations in specific ion-exchange mechanisms and the distinct characteristics of surface interactions for each species. NH4+ benefits from strong electrostatic attraction and complexation with groups that come from tannins. In contrast, nitrate might be more prone to obstruction or influence from competition during the desorption phase. These findings highlight the need for enhanced optimization of the regeneration protocols to maintain high adsorption efficiency over extended use. The capacity of T-HPB to retain a substantial fraction of its initial efficacy after numerous cycles substantiates its viability as a sustainable and economical adsorbent for the concurrent elimination of nitrogenous pollutants.

3.2.7 Selectivity and Effect of Competing Ions

The selectivity of T-HPB for NH_4^+ and NO_3^- amidst prevalent co-existing ions was assessed to replicate actual wastewater conditions. Figure 15 depicts the capacity retention percentages of T-HPB in comparison to various competing ions, including chloride (Cl^-), sulfate (SO_4^{2-}), calcium (Ca^{2+}), and magnesium (Mg^{2+}). The experimental results indicate that the highest retention occurred in the presence of chloride and sulfate, succeeded by calcium and magnesium. The substantial retention of nitrogen species in the presence of chloride and sulfate highlights the biochar's enduring adsorption capacity in the context of common anionic species present in

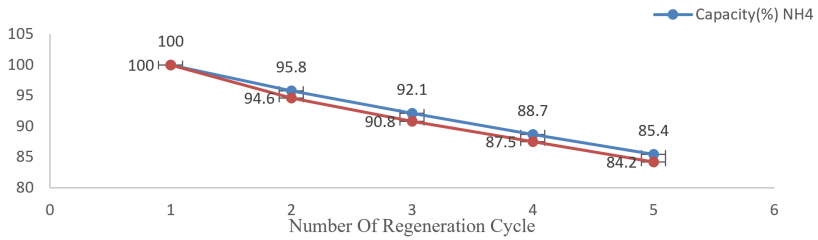

Figure 14 The reusability of T-HPB for NH_4^+ and NO_3^-

wastewater. This illustrates the robust performance and potential effectiveness of the tannin-functionalized hierarchical porous structure in complex wastewater matrices. A minor reduction in retention was observed with calcium and magnesium, indicating a slight competitive effect from divalent cations; however, the material's overall capacity remains strong. These findings underscore the material's suitability for practical applications in nitrogen-rich wastewater treatment, where competing ions are often present. The pronounced selectivity of T-HPB is due to the specific interactions between the functional ligands on the biochar surface and the target ions, which significantly reduce the interference from non-target species. This attribute is essential for the creation of effective and dependable adsorbents for environmental remediation.

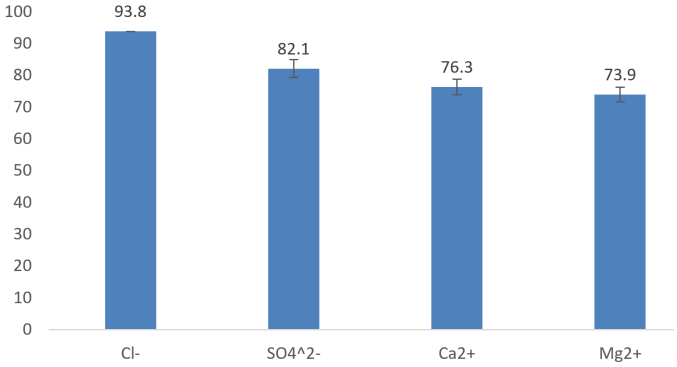

Figure 15 The capacity retention percentages of T-HPB against several competing ions

3.3 Proposed Mechanism

The adsorption of NH_4^+ and NO_3^- onto tannin-functionalized hierarchical porous biochar (T-HPB) transpires via a multi-modal synergistic mechanism, shaped by the unique architecture of the lignocellulosic framework and the abundant polyphenolic groups. The mechanistic schematic (Figure 16) illustrates that the adsorption process initiates with rapid film diffusion of ions into the macroporous channels, followed by intra-particle diffusion through the interconnected meso-microporous framework, which provides a significant active surface area exceeding 450 m2/g. The process of ammonium removal was chiefly enabled by cation exchange and surface complexation. The introduction of tannin molecules led to an excess of vicinal hydroxyl (-OH) and carboxyl (-COOH) groups, which underwent deprotonation at the experimental pH of 7.0, resulting in a negatively charged surface. The electrostatic attraction between the cationic ammonium species and the anionic oxygen-containing functional groups made it easier for the first docking to happen. So, the higher density of phenolic rings created localized pi-electron domains, which boosted cation-pi interactions and made NH_4^+ ions more stable in the carbon matrix. The adsorption of nitrate exhibited a unique and complementary pattern characterized by hydrogen bonding and anion-pi interactions. Notwithstanding the net negative surface charge of the biochar at neutral pH, the existence of protonated amine residues from the tannin-protein complexes and the development of water-bridged complexes facilitated localized binding of nitrate. The nitrogen-rich functionalities on the T-HPB surface functioned as hydrogen bond donors to the oxygen atoms of the NO3- trigonal planar structure, with a calculated binding energy indicating robust physisorption. Moreover, the hierarchical porosity significantly contributed to alleviating the competitive influences of co-existing ions. The size-exclusion characteristics of the narrow micropores facilitated the ingress of smaller hydrated radii of ammonium (1.61 Å) and nitrate (1.79 Å), whereas larger multivalent ions were partially barred from the most profound active sites. The pH-dependent characteristics of the system offered additional understanding of the interfacial chemistry. Below the point of zero charge (PZC = 5.4), nitrate adsorption was augmented due to significant protonation of surface sites,

resulting in a positive zeta potential of +12.4 mV, which intensified the electrostatic attraction for NO_3^-. In contrast, ammonium adsorption reached its zenith at pH levels ranging from 6.0 to 8.0, where the deprotonation of carboxylic acid groups (pKa $\approx$ 3.5–5.0) was fully realized, thereby optimizing the cation exchange capacity. Tannin played a crucial role in inhibiting the leaching of captured ions; the establishment of stable surface complexes through bidentate or polydentate coordination with polyphenolic ligands guaranteed that both ammonium and nitrate remained sequestered, even amid varying ionic strength conditions. This dual-functionalized surface chemistry, connecting hydrophobic carbon layers with hydrophilic organic ligands, facilitated the concurrent and prolonged entrapment of nitrogen species via a synergistic ion-exchange and complexation mechanism. Table 4 illustrates that the developed T-HPB exhibits superior or competitive adsorption performance relative to recently reported biochar-based materials, especially in the removal of NO_3^-–N, underscoring the efficacy of tannin functionalization in improving dual-ion adsorption.

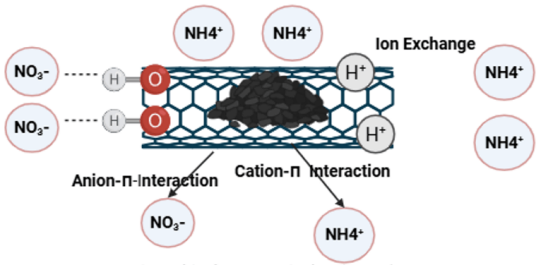

Figure 16 Hierarchical Porous Biochar (T-HPB)

Table 4 Comparison of T-HPB performance with other reported materials

Material	Target Pollutant	Optimal Conditions (pH, Time, Temp)	Maximum Capacity (mg/g)	Reference
Tannin-functionalized HPB (T-HPB)	NH_4^+–N / NO_3^-–N	6.5, 120 min, 25°C	78.4/ 52.1	This study
Biochar (various feedstocks)	NH_4^+–N / NO_3^-–N	6–7, 120–240 min, 25°C	20–35 / 10–25	[34]
Nitrate adsorption on biochar	NO_3^-–N	~7, 180 min, 25°C	15–30	[35]
Fe/N-modified biochar	NO_3^-–N	5–6, 180 min, 25°C	20–35	[36]
Biochar (different feedstocks)	NO_3^-–N	6–7, 120–300 min, 25°C	12–28	[37]
Biochar (pyrolysis-temp dependent)	NH_4^+–N / NO_3^-–N	6–8, 120–180 min, 25°C	18–40 / 10–30	[38]
Modified biochar	NH_4^+–N	7, 120 min, 25°C	25–38	[28]
Composite biochar system	NH_4^+–N / NO_3^-–N	6–7, 180–240 min, 25°C	20–36 / 15–28	[39]

4 Conclusion

This study effectively illustrated the synthesis of tannin-functionalized hierarchical porous biochar (T-HPB) obtained from lignocellulosic residues via a coordinated approach involving phosphoric acid activation and surface grafting. The characterization results confirmed the development of a complex pore structure with a specific surface area of 842.6 m^2/g and the successful incorporation of polyphenolic moieties, significantly increasing the density of surface oxygen-containing functional groups. The T-HPB demonstrated remarkable simultaneous removal efficacy at optimal conditions, specifically at a pH of 6.5 and a temperature of 25°C. The greatest adsorption capacities attained were 78.4 mg/g for ammonium and 52.1 mg/g for nitrate. Mechanistic investigations revealed that the removal process is augmented by a synergistic interplay of electrostatic attraction, surface complexation with tannin hydroxyl groups, and enhanced ion-exchange pathways within the hierarchical macro-mesopore architecture. Furthermore, the material retained over 85% of its initial capacity after five regeneration cycles, demonstrating its stability and reusability in complicated wastewater matrices. T-HPB, due to its exceptional performance and economical precursor source, offers a sustainable and effective solution for nutrient remediation in aquatic environments. Future research should concentrate on pilot-scale continuous flow systems and the subsequent application of nutrient-rich biochar as a slow-release fertilizer to foster a circular economy and complete the nutrient cycle in agricultural practices.

Conflicts of Interest

The authors declare that they have no conflicts of interest.

Acknowledgements

This work was supported by the Deanship of Scientific Research, Vice Presidency for Graduate Studies and Scientific Research, King Faisal University, Saudi Arabia [Grant No. KFU262099].

References

[1] Aman Prakash, Sofia Khanam. Nitrogen Pollution Threat to Mariculture and Other Aquatic Ecosystems: An Overview. Journal of Pharmacy and Pharmacology. 2021, 9(12). https://doi.org/10.17265/2328-2150/2021.12.005

[2] Kuriyama K, Hayashi K. Sustainable Agriculture and the Nitrogen Issue. Economics of Sustainable Agriculture. Published online 2025: 1-10. https://doi.org/10.1007/978-981-96-3502-3_1

[3] Wang Z, Zhang L, Zeng W, et al. A loading rate switch strategy for stable nitritation in mainstream municipal wastewater. Nature Sustainability. 2024, 7(3): 305-314. https://doi.org/10.1038/s41893-024-01276-z

[4] Zhou Y, Zhu Y, Zhu J, et al. A Comprehensive Review on Wastewater Nitrogen Removal and Its Recovery Processes. International Journal of Environmental Research and Public Health. 2023, 20(4): 3429. https://doi.org/10.3390/ijerph20043429

[5] Ojo OE, Oludolapo OA. Innovative Recovery Methods for Metals and Salts from Rejected Brine and Advanced Extraction Processes—A Pathway to Commercial Viability and Sustainability in Seawater Reverse Osmosis Desalination. Water. 2025, 17(21): 3141. https://doi.org/10.3390/w17213141

[6] Khandaker T, Islam T, Nandi A, et al. Biomass-derived carbon materials for sustainable energy applications: a comprehensive review. Sustainable Energy & Fuels. 2025, 9(3): 693-723. https://doi.org/10.1039/d4se01393j

[7] Luo L, Li J, Xing Z, et al. Biochar for Mitigating Nitrate Leaching in Agricultural Soils: Mechanisms, Challenges, and Future Directions. Water. 2025, 17(17): 2590. https://doi.org/10.3390/w17172590

[8] Guan X, Zhang B, Wang Z, et al. Natural polyphenol tannin-immobilized composites: rational design and versatile applications. Journal of Materials Chemistry B. 2023, 11(21): 4619-4660. https://doi.org/10.1039/d3tb00661a

[9] Wu W, Wang Y, Hu X. Mass transfer driven pore engineering of activated carbon from the activation of biomass. Green Chemistry. 2026, 28(8): 3486-3511. https://doi.org/10.1039/d5gc05946a

[10] Rowell C, Lam EY. Mobile-Phone Antenna Design. IEEE Antennas and Propagation Magazine. 2012, 54(4): 14-34. https://doi.org/10.1109/map.2012.6309152

[11] Takabi AS, Shirani M, Semnani A. Apple stem as a high performance cellulose based biosorbent for low cost and eco-friendly adsorption of crystal violet from aqueous solutions using experimental design: Mechanism, kinetic and thermodynamics. Environmental Technology & Innovation. 2021, 24: 101947. https://doi.org/10.1016/j.eti.2021.101947

[12] He X, Zheng N, Hu R, et al. Hydrothermal and Pyrolytic Conversion of Biomasses into Catalysts for Advanced Oxidation Treatments. Advanced Functional Materials. 2020, 31(7). https://doi.org/10.1002/adfm.202006505

[13] Jia W, Yu Z, Chen J, et al. Synergistic effect between biochar and nitrate fertilizer facilitated arsenic immobilization in an anaerobic contaminated paddy soil. Science of The Total Environment. 2024, 955: 177007. https://doi.org/10.1016/j.scitotenv.2024.177007

[14] Mao Y, Liu J, Lin Q, et al. Efficient removal of Cr(VI) and bisphenol A by a tannic acid-functionalized porous biochar. Materials Chemistry and Physics. 2024, 326: 129770. https://doi.org/10.1016/j.matchemphys.2024.129770

[15] Wang T, Xue L, Zheng L, et al. Biomass-derived N/S dual-doped hierarchically porous carbon material as effective adsorbent for the removal of bisphenol F and bisphenol S. Journal of hazardous materials. 2021, 416: 126126. https://doi.org/10.1016/j.jhazmat.2021.126126

[16] Zhang M, Song G, Gelardi DL, et al. Evaluating biochar and its modifications for the removal of ammonium, nitrate, and phosphate in water. Water Research. 2020, 186: 116303. https://doi.org/10.1016/j.watres.2020.116303

[17] Yao Y, Gao B, Zhang M, et al. Effect of biochar amendment on sorption and leaching of nitrate, ammonium, and phosphate in a sandy soil. Chemosphere. 2012, 89(11): 1467-1471. https://doi.org/10.1016/j.chemosphere.2012.06.002

[18] Elbana M, Gamal R, El-Shirbeny MA, et al. Mesoporous biochar reshapes soil water dynamics under shallow groundwater: interactions with nitrogen management. Frontiers in Soil Science. 2025, 5: 1718929.
https://doi.org/10.3389/fsoil.2025.1718929
[19] Liu T, Fan X, Wu K, et al. Structural characteristics of biochars made from different parts of corn straw and their adsorption performances for methylene blue. Journal of Water Process Engineering. 2024, 68: 106562.
https://doi.org/10.1016/j.jwpe.2024.106562
[20] Leng L, Xiong Q, Yang L, et al. An overview on engineering the surface area and porosity of biochar. Science of The Total Environment. 2021, 763: 144204.
https://doi.org/10.1016/j.scitotenv.2020.144204
[21] Raveendran K. Pyrolysis characteristics of biomass and biomass components. Fuel. 1996, 75(8): 987-998.
https://doi.org/10.1016/0016-2361(96)00030-0
[22] Yang H, Yan R, Chen H, et al. Characteristics of hemicellulose, cellulose and lignin pyrolysis. Fuel. 2007, 86(12-13): 1781-1788.
https://doi.org/10.1016/j.fuel.2006.12.013
[23] Brebu M, Vasile C. Thermal degradation of lignin–a review. Cellulose Chemistry & Technology. 2010, 44(9): 353.
[24] Hatakeyama T, Hatakeyama H. Thermal properties of green polymers and biocomposites. Dordrecht: Springer Netherlands, 2004.
[25] Das C, Tamrakar S, Kiziltas A, et al. Incorporation of Biochar to Improve Mechanical, Thermal and Electrical Properties of Polymer Composites. Polymers. 2021, 13(16): 2663.
https://doi.org/10.3390/polym13162663
[26] Aboughaly M, Babaei-Ghazvini A, Dhar P, et al. Enhancing the potential of polymer composites using biochar as a filler: a review. Polymers. 2023, 15(19): 3981.
https://doi.org/10.3390/polym15193981
[27] Zhu Y, Liu S, Chen H, et al. Evaluating biochar for adsorption of ammonium nitrogen in wastewater: insights into modifications and mechanisms. Environmental Research. 2025, 277: 121615.
https://doi.org/10.1016/j.envres.2025.121615
[28] Chang H, Yang X-y, Liang D, et al. Enhanced removal of ammonium nitrogen from aqueous solutions using a novel biochar derived from millet shells through both static adsorption and dynamic column experiments. Journal of Water Process Engineering. 2024, 58: 104848.
https://doi.org/10.1016/j.jwpe.2024.104848
[29] Wang H, Chen Q, Liu R, et al. Enhanced removal performance and mechanism of NH4+/NO3- in Starch-FeS-biochar-amended vertical flow constructed wetlands under Pb stress. Journal of Water Process Engineering. 2023, 55: 104170.
https://doi.org/10.1016/j.jwpe.2023.104170
[30] Nguyen V-T, Vo T-D-H, Tran T, et al. Biochar derived from the spent coffee ground for ammonium adsorption from aqueous solution. Case Studies in Chemical and Environmental Engineering. 2021, 4: 100141.
https://doi.org/10.1016/j.cscee.2021.100141
[31] Wu J, Li K, Zhao Z. Innovative nitrogen-doped biochar-derived ball-milled defective in-situ amino biochar molecularly imprinted gels for selective removal of BPA: Theoretical simulation and mechanistic insights. Chemical Engineering Journal. 2025, 509: 161338.
https://doi.org/10.1016/j.cej.2025.161338
[32] Zhang G, Huang F, Shi Y, et al. Integration of experimental and computational techniques to elucidate the Cu(II) adsorption mechanisms of nitrogen-doped chitosan microsphere biochars. Chemical Engineering Journal. 2025, 521: 166840.
https://doi.org/10.1016/j.cej.2025.166840
[33] Berlin M, Suresh Kumar G. Numerical modelling on sorption kinetics of nitrogen species in wastewater-applied agricultural field. Applied Water Science. 2018, 8(8).
https://doi.org/10.1007/s13201-018-0869-5
[34] Trazzi PA, Vashishtha M, Najser J, et al. Adsorption of Ammonium, Nitrate, and Phosphate on Hydrochars and Biochars. Applied Sciences. 2024, 14(6): 2280.
https://doi.org/10.3390/app14062280
[35] He Z, Wang C, Cao H, et al. Nitrate absorption and desorption by biochar. Agronomy. 2023, 13(9): 2440.
https://doi.org/10.3390/agronomy13092440
[36] Haghighi Mood S, Pelaez-Samaniego MR, Han Y, et al. Iron- and Nitrogen-Modified Biochar for Nitrate Adsorption from Aqueous Solution. Sustainability. 2024, 16(13): 5733.
https://doi.org/10.3390/su16135733
[37] Eissa R, Jeyakumar L, McKenzie DB, et al. Influence of Biochar Feedstocks on Nitrate Adsorption Capacity. Earth. 2024, 5(4): 1080-1096.
https://doi.org/10.3390/earth5040055
[38] Kohira Y, Fentie D, Lewoyehu M, et al. Elucidation of ammonium and nitrate adsorption mechanisms by water hyacinth biochar: effects of pyrolysis temperature. Environmental Science and Pollution Research. 2024, 32(2): 762-782.
https://doi.org/10.1007/s11356-024-35808-z
[39] Chang J-H, Sivasubramanian P, Dong C-D, et al. Study on adsorption of ammonium and nitrate in wastewater by modified biochar. Bioresource Technology Reports. 2023, 21: 101346.
https://doi.org/10.1016/j.biteb.2023.101346